JOURNAL OF MATERIALS SCIENCE 25 (1990) 4856–4865

Reactions at the $Al/SiO_2/SiC$ layered interface

A. E. HUGHES, M. M. HEDGES, B. A. SEXTON
CSIRO, Division of Materials Science and Technology, Locked Bag 33, Clayton, Vic., 3168, Australia

Electron spectroscopy and thermodynamic modelling have been used to examine reactions at the $Al/SiO_2/SiC$ layered interfaces at 800° C. The reactions have been examined as a function of oxide thickness. Three regimes have been isolated: (i) where there is no oxide present aluminium and SiC react to produce Al_4C_3 and free silicon; (ii) where there is a thin oxide present the initial products are aluminosilicates and amorphous alumina; however, once the SiO_2 is consumed, Al_4C_3 emerges as a product; (iii) where a thick oxide is present only aluminosilicate and alumina are formed.

1. Introduction

Silicon Carbide (SiC) is a material which has application in such diverse fields as electronics [1] and materials science and engineering [2].

In the area of electronics, for example, silicon carbide's wide band gap, chemical inertness and thermal stability make it a good prospective semiconductor material. Two of the more attractive areas for silicon carbide devices are in the fabrication of blue light emitting diodes [3, 4] where aluminium is diffused into the SiC and acts as an acceptor dopant level, and the fabrication of metal–oxide semiconductor devices (MOS) constructed from $Al–SiO_2–SiC$ layers [5].

In materials science, SiC is of interest as a light, strong and tough non-oxide ceramic [6]. Its diversity in materials science also extends to composite materials as well, where SiC particles, fibres and powders may be used to reinforce other materials such as aluminium [7] or Al_2O_3 [8].

The production of good composite materials relies heavily on the nature of the interfacial bonding between the reinforcing material and the matrix [9]. The surface of SiC is generally quite different from the bulk. The SiC may have surface layers consisting of specialized finishes [10] or native oxides [11, 12]. The reaction of these surface layers with the matrix material may result in the production of unwanted interfacial reaction products which are detrimental to the mechanical properties of the composite. One such reaction product in the Al/SiC system is Al_4C_3 which has a tendency to corrode with a resultant diminution of the mechanical properties [13].

In previous studies of the Al/SiC interface apparently conflicting conclusions have been drawn about the presence of interfacial reaction products such as Al_4C_3. Arsenault and Pande [14], using Auger electron spectroscopy (AES) and STEM/EDAX found that aluminium diffused into SiC fibres without the formation of Al_4C_3. Bermundez [15] and Porte [16] using AES and X-ray photoelectron spectroscopy (XPS) both observed the formation of Al_4C_3 when heating single crystal (0 0 0 1) α-SiC to 600° C after aluminium had been evaporated on to the crystal. Iseki *et al.* [17] examined the reaction between aluminium and SiC in sintered bodies by TEM and observed the formation of Al_4C_3. They also observed, however, that the presence of liquid silicon decreased the amount of Al_4C_3 that formed.

Apart from some work on MOS devices thermally treated below 500° C [18], no work has been reported on the effects of an oxide layer on the $Al/SiO_2/SiC$ interfacial reactions between 500 and 1000° C.

The current study examines the reaction between aluminium, SiO_2 and SiC in the $Al/SiO_2/SiC$ system at 800° C with a view to understanding the interfacial chemistry pertinent to the problem of reinforcing aluminium with SiC. XPS and X-ray generated Auger spectroscopy (XAES) were employed to examine the interfacial reactions between aluminium and SiC in the presence of varying thicknesses of SiO_2. In addition, thermodynamic modelling was used to predict the equilibrium assemblage of reaction products as a function of aluminium addition and silica content. The predicted equilibrium assemblages were used to assist in the identification of species observed in the XPS experiments. Elucidation of the interfacial reaction chemistry could ultimately lead to better tailoring of parameters for the industrial processing of composite materials.

2. Experimental procedure

2.1. Specimen preparation

Single crystals of SiC, obtained from Electroschmelzwerk Kempton (West Germany), were identified by X-ray diffraction as 6H–SiC [19]. Crystals of the required size were cut with a diamond saw and polished with 6 μm diamond paste. Oxide layers were generated in air, by thermal oxidation in a muffle furnace at 600° C [20]. The SiC crystal was then mounted on to a platinum foil attached by tantalum heating leads to high current copper leads. Heating of the crystal was achieved by resistively heating the platinum foil and the temperature was monitored by a K-type thermocouple spot welded to the platinum foil. The heating probe, the platinum foil and the SiC single crystal were liquid nitrogen cooled in order to

0022-2461/90 $03.00 + .12 © *1990 Chapman and Hall Ltd.*

minimize the evolution of contaminating gases such as CO_2 during the reaction experiments. Aluminium was evaporated under ultra-high vacuum on to the crystal surface from a tantalum filament. The amount of aluminium evaporated for each experiment was monitored by examining the attenuation of the SiC Si2p XPS line. When the Si2p was reduced by 0.6 of its original intensity the aluminium evaporation was stopped. This resulted in approximately 1 nm of aluminium being evaporated into the SiO_2/SiC system.

The reference amorphous Al_2SiO_5 was prepared by co-precipitation using silicon and aluminium alkoxides as starting materials. Tetraethoxysilane (Pfaltz and Bauer Inc.) was hydrolysed at 70° C for 48 h. Aluminium tri-sec-butoxide (Aldrich) was mixed with butanol at 70° C. The two solutions were mixed, stirred for 72 h at 70° C then filtered, washed and dried at 100° C in air. Analytical grade Al_4C_3 was obtained from CERAC.

2.2. Spectroscopy

X-ray photoelectron spectra were measured in a Vacuum Generators ESCALAB at a vacuum of 5 to 7×10^{-10} torr (1 torr = 133.322 Pa) using both Al$K\alpha$ (1486.6 eV) and Mg$K\alpha$ (1253.6 eV) X-rays. Photoemission binding energies (BE) were referred to the Fermi level. Auger spectra were measured using Bremsstrahlung X-radiation [21]. Atom number ratios were calculated using the formula

$$\frac{N_A}{N_B} = \frac{I_A \sigma_B}{I_B \sigma_A} \qquad (1)$$

where N_A and N_B are the number of atoms of species A and B, I_A and I_B are the integral intensity of species A and B, and σ_A and σ_B are the photoionization cross-sections, respectively [22]. Individual spectral components were resolved from complex spectral envelopes using a curve-fitting technique described by Hughes and Sexton [23]. Prior to curve fitting, all spectra were smoothed using Savitsky–Golay smoothing [24, 25] and background subtracted using a non-linear background described by Procter and Sherwood [26]. Spectra were then fitted used a Gaussian–Lorentzian product function.

The film thicknesses for the silica and aluminium overlayers were determined by the equation [27]

$$d = K \ln(1 + MR_{\text{film/substrate}}) \qquad (2)$$

where the coefficient $K = \lambda/\cos(\theta)$, θ = angle of detection (70°) and λ is the inelastic mean free path as determined by the method of Tanuma *et al.* [28]. $R_{\text{film/substrate}}$ is the ratio of the intensities from the film and support, M is the ratio of intensities from an infinitely thick support and infinitely thick film, i.e. the ratio of intensities from the pure materials. M for the oxide thickness determination had a value of 1.0237 and K had values of 29.986 (Al$K\alpha$) and 25.828 (Mg$K\alpha$). For the aluminium film thickness the values of $R_{\text{film/substrate}}$ are given in Table I, and the values of K were 20.3 (Al$K\alpha$) and 18.57 (Mg$K\alpha$).

2.3. Thermodynamic modelling

Thermodynamic analysis of the interfacial reactions occurring in the system Al/SiO_2/SiC were performed using the program "CHEMIX" of the CSIRO Thermochemistry System [29]. Equilibrium compositions were computed using the well-known method of Gibbs energy minimization. Details of the experiment are described in Section 3.3. The basic thermodynamic data sets for all species in the system were taken from the JANAF file contained in the THERMODATA data bank. The important species considered were: SiO(g), AlO(g), Al_2O(g), CO(g), Si_2(g), Si_3(g) and Si_2C(g) (gas phase); Al(l), Si(l), SiO_2(l), and Al_2O_3(l) (liquid phase) and Al(s), Al_4C_3(s), Al_2O_3(s) (α-, γ-, δ-, κ-alumina), Al_2SiO_5(s) (andalusite, kyanite and sillimanite), $Al_6Si_2O_{13}$(s) (mullite), Si(s), SiC(α- and β-silicon carbide) and SiO_2(s) (quartz and cristobalite) (solid phase). The liquid phase was assumed to be an ideal solution (i.e. component activities were equal to their mole fractions) and the solids were assumed to be pure single phases and any possible solid solutions were not considered.

3. Results

3.1. XPS analysis

3.1.1. Spectroscopic results

Quantitative analyses, presented later, were obtained from curve fitting the Si2p and Al2p photoemission lines. Atom number ratios were calculated from the integral areas obtained from two- and three-component fits to the spectra. In Fig. 1 the different species present after reacting aluminium with a thin (d = 1.8 nm) silicon oxide film on SiC (designated Al/SiO_2 (d = 1.8 nm)/SiC) for 120 min at 800° C have been resolved by three-component fits to the Si2p and Al2p spectra. The justification for employing a three-component fit comes from inspection of the Auger lines in Fig. 2 obtained for the same experiment as the data depicted in Fig. 1. Three peaks are evident in both the Si(KLL) (Fig. 2a) and Al(KLL) (Fig. 2b) spectra indicating that three distinct chemical species are present at the reacted interface for the silicon and aluminium.

TABLE I Estimates of molar ratios of reactants*

Experiment	Depth SiC (nm)	SiC (10^8 mol)	Molar ratios (SiC–1.0) Al : SiO_2 : SiC
I	9.03	7.23	0.134 : 0.0 : 1.0 (no oxide)
II	8.06	6.46	0.16 : 0.054 : 1.0
III	7.27	5.82	0.194 : 0.106 : 1.0
IV	7.43	5.95	0.129 : 0.118 : 1.0 (thin oxide)
V	3.97	3.18	0.258 : 0.629 : 1.0 (thick oxide)

*Assuming 100 nm analysis depth.

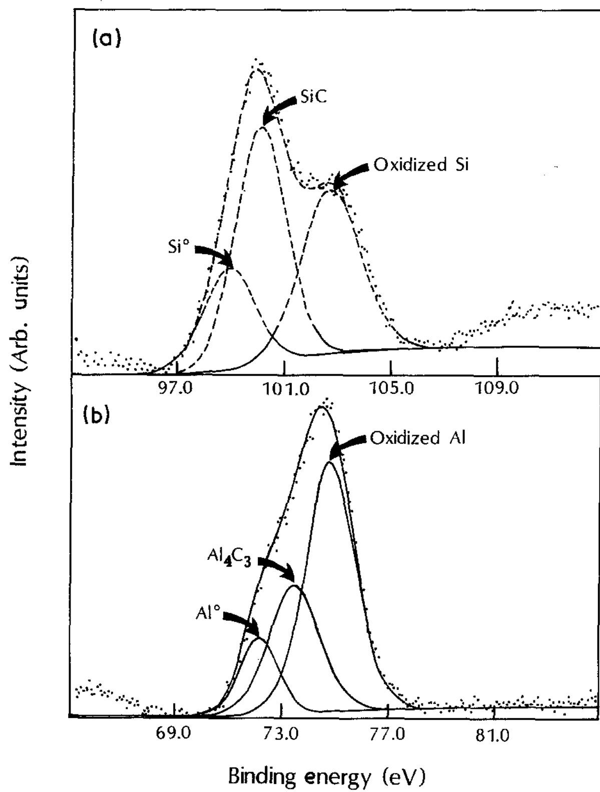

Figure 1 Examples of the extraction of the phase intensities by curve-fitting photoemission lines. The diagram displays three-component fits to (a) the Si2p and (b) the Al2p peaks for the system Al/SiO_2 (d = 1.8 nm)/SiC, 120 min, 800° C.

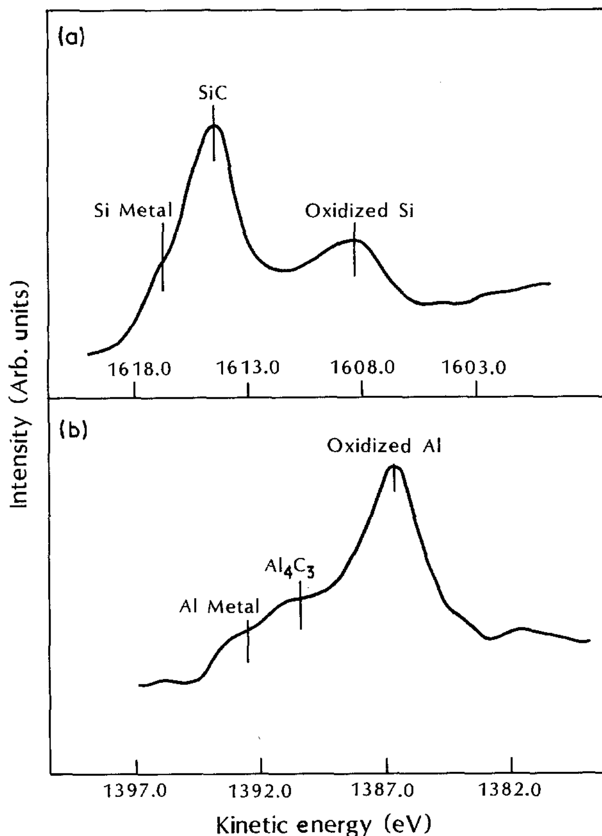

Figure 2 (a) Si(KLL) and (b) Al(KLL) Auger lines after 120 min reaction at 800° C. Chemical shifts in the Auger lines are larger than the corresponding shifts in the photoemission lines. Both the Si(KLL) and Al(KLL) lines clearly display three different components.

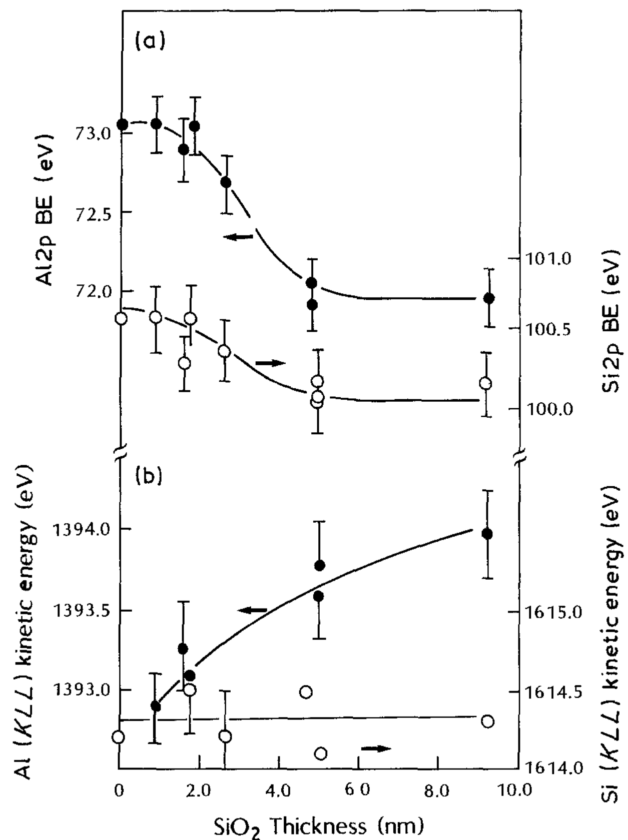

Figure 3 Photoemission and Auger line shifts as a function of oxide thickness for the unreacted surface. (a) Al2p and Si2p binding energies, (b) Al(KLL) and Si(KLL) kinetic energies. The decrease in the Si2p binding energy in the absence of any Si(KLL) shift is indicative of band-bending and Fermi level shifts. The shifts in the Al2p binding energy and the Al(KLL) kinetic energy are the result of dipole production within the SiO_2 layer.

Having extracted the components from curve fitting the Al2p and Si2p photoemission lines, it is necessary to correlate each component with a phase present at the reacted interface. Two phenomena which complicate the assignment of the components to particular phases are band-bending and Fermi level shifts which may result from doping of SiC with aluminium [30, 31] or surface oxidation [32]. Consequently, it must be established whether photoemission BE shifts are chemical or electronic in origin.

Band-bending and Fermi level shifts should manifest themselves as a shift of the Si2p "SiC" component as a function of oxide thickness [31]. The Auger lines, however, should be independent of both effects and hence the oxide thickness. In Fig. 3 the Si2p "SiC" component, the evaporated metal Al2p component (before reaction) and the corresponding Auger lines are plotted as a function of oxide thickness. The Si2p "SiC" (Fig. 3a) component exhibits a decrease of 0.5 eV as a function of the oxide thickness up to 4.0 nm oxide. This shift indicates that the bands near the surface are bent towards the Fermi level by up to 0.5 eV with increasing oxide thickness. Confirmation that the Si2p shift is electronic in nature is provided by the absence of any shift in the Si (KLL) line over the range of oxide thicknesses examined here (Fig. 3b). The shift in the Si2p level is the result of a potential being set up at the SiO_2/SiC interface during oxidation. Kee *et al.* [34] have suggested that a conducting

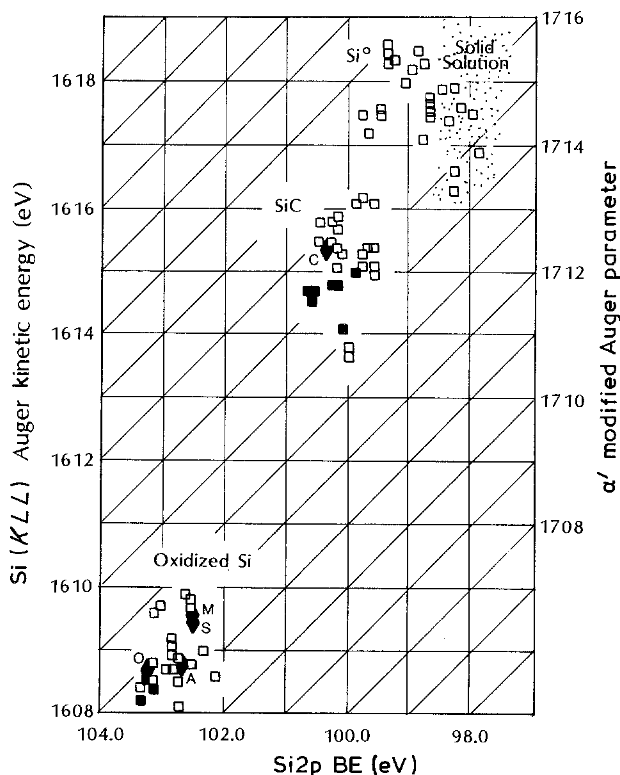

Figure 4 Two-dimensional chemical state plot for the silicon reaction products. The Si(KLL) Auger kinetic energy has been plotted as a function of the Si2p binding energy. All the data plotted are referenced to the Fermi level. Three regions are indicated: (i) Oxidized silicon, (ii) SiC, and (iii) Si^0. The spread of data in all three regions has different physical origins. Spreading occurs in the "Oxidized" region due to the presence of SiO_2 as well as aluminosilicate, in the SiC region because as the reaction proceeds the SiC becomes silicon-rich and in the Si^0 region as a result of a range of environments from true Si^0 to silicon in solid solution with aluminium (indicated by the hatched area). (◆) Reference compounds: A, amorphous Al_2SiO_5; C, SiC; O, SiO_2; M, mullite; S, sillimanite. The dark rectangles represent the species at the unreacted interface.

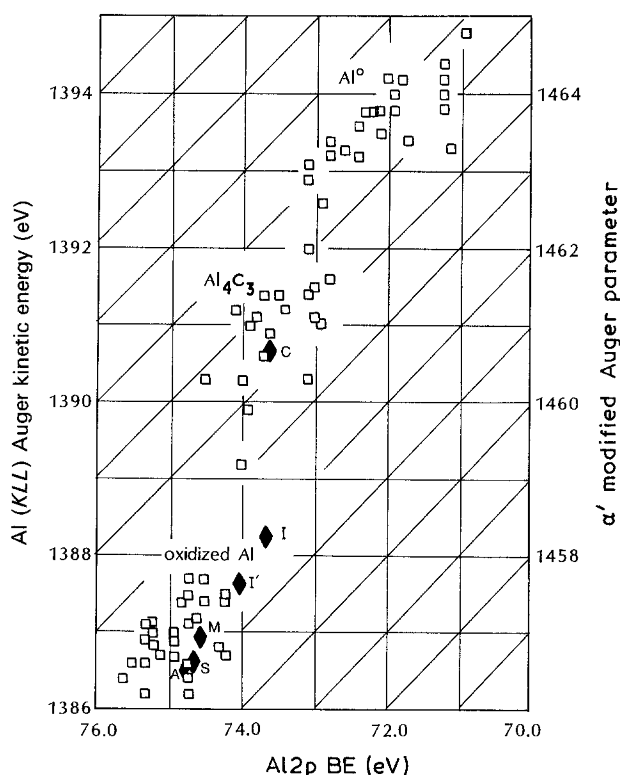

Figure 5 Two-dimensional chemical state plot for the aluminium reaction products. The Al(KLL) Auger kinetic energy has been plotted against the Al2p photoemission binding energy. All data have been referenced to the Fermi level. Three regions are indicated: (i) oxidized aluminium, (ii) Al_4C_3 and (iii) Al^0. The spread of the results in the oxidized aluminium region is due to the presence of Al_2O_3 as well as aluminosilicate. The spread in the Al^0 region is due to the presence of an interfacial dipole in the SiO_2 layer as discussed in the text. (◆) Reference compounds: A, amorphous Al_2SiO_5; C, Al_4C_3; I, α-Al_2O_3; I′, oxide layer on aluminium (amorphous alumina); M, mullite; S, sillimanite.

layer may be generated at the interface which shields the SiC. They suggest that the conducting layer may be comprised of free carbon generated at the interface or free silicon in the SiO_2 layer or ionized CO and CO_2 at the interface.

The aluminium component, however, exhibits a marked decrease from 73.0 to 72.0 eV (Fig. 3a) and the Al (KLL) line shows an increase (Fig. 3b) as a function of increasing thickness of oxide. One possible explanation of this behaviour is provided by the presence of a dipole within the oxide layer resulting in a net negative charge at the Al/SiC interface [35]. Presumably the reason that the decrease of the Al2p BE only manifests itself at oxide thicknesses of about 2.0 nm is due to patchy or very thin oxides at thicknesses less than 2.0 nm which allows current flow from the aluminium to SiC, neutralizing the dipole.

Having isolated photoemission BE shifts due to electronic effects, other shifts may now be interpreted as chemical shifts. Figs 4 and 5 summarize the spectroscopic results for silicon and aluminium in the form of two-dimensional chemical state plots for silicon and aluminium compounds. The two-dimensional chemical state plot, in which the Auger (KLL) kinetic energy is plotted against the 2p photoemission BE, provides a two-dimensional spectroscopic map of compounds of the element of interest [36]. In Fig. 6, BE splittings of the C1s–Si2p (Fig. 6a), O1s–Al2p (Fig. 6b) and O1s–Si2p lines (Fig. 6c) are plotted as a function of reaction time at 800° C. Presentation of the XPS data in the form of photoemission BE splittings has previously been used by other authors to circumvent band-bending phenomena [16, 37].

For the unreacted interface the silicon data fall into two distinct regions labelled "SiC" (100.4 eV) and "oxidized Si" (103.3 eV) (dark squares) on the two-dimensional chemical state plot of Fig. 4. There was no evidence from the photoemission data for the presence of silicon oxycarbide [38]. The O1s–Si2p "oxidized Si" splitting of 429.5 eV plotted in Fig. 6c is indicative of a disordered or amorphous oxide. Jorgensen *et al.* [39] have previously observed by XRD that oxides grown on SiC below 1200° C are amorphous in agreement with BE splitting of 429.5 eV. A similar situation exists with oxide films grown on silicon; Sun *et al.* [40], in an extensive study of the Si/SiO_2 interface, measured an O1s–Si2p splitting of 429.5 eV for highly disordered oxides.

Disorder is also observed in the SiC surface because the C1s–Si2p (Fig. 6a) splitting has an average value of approximately 183.2 eV which Porte [16] has indicated is typical of disordered SiC surfaces, where the disorder has been induced by argon ion bombardment. The disorder at the SiC/SiO_2 interface, in the current experiments, may well be explained by the

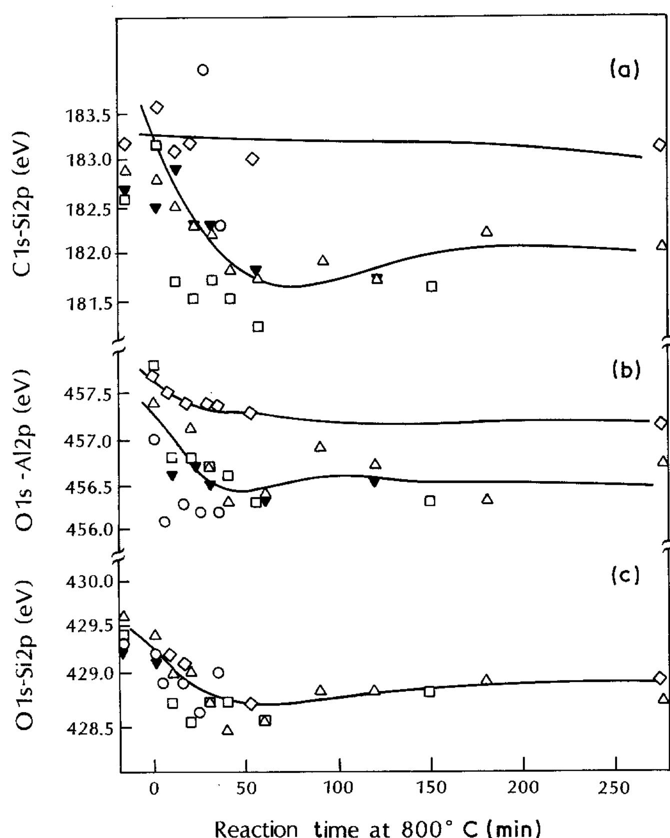

Figure 6 Photoemission binding energy splittings as a function of the reaction time at 800° C. (a) C1s–Si2p, (b) O1s–Al2p, (c) O1s–Si2p. Data for the following oxide thicknesses are presented: (▼) 0.0 nm, (○) 0.87 nm, (△) 1.8 nm, (□) 2.0 nm, (◇) 5.1 nm. The relevance of the splittings are discussed in the text and displayed in Table II.

presence of reaction products from the oxidation such as those proposed by Kee *et al.* [34].

The aluminium which is evaporated as metal is labelled "Al^0" on the two-dimensional chemical state plot for the aluminium reaction data (Fig. 5). A small amount of oxide was also present after evaporation which was fairly amorphous, as indicated by the O1s–Al2p splitting of approximately 457.5 eV [36].

After reaction at 800° C a number of notable changes are apparent as a function of time, on both the silicon and aluminium two-dimensional chemical state plots (Figs 4 and 5) and the binding energy splitting of Fig. 6. In Fig. 4 for the silicon data, reaction at 800° C produces the group labelled "Si^0" on the plot. The spread of the "Si^0" region, bordered by 97.5 to 99 eV Si2p BE and 1617.0 eV Si (*KLL*) kinetic energy, delineates a regime where silicon is in solid solution with aluminium. The XPS experiments were carried out at room temperature where no liquid phases exist. At 800° C we assume that the room-temperature solid solution has melted to form a liquid solution. The solid solution regime is approximately 1 eV below the normal silicon metal position but is in agreement with the predictions of a negative 0.7 eV shift given by del Guidice *et al.* [41] and the observation by Brillson *et al.* [42] of a 1 eV shift to lower BE for silicon in the Al/cleaved Si(1 1 1) system. The spread of the results is probably indicative of the extent of solid solution.

The SiC region also changes as a function of reaction time. The change is manifested by a shift of the "centre of mass" of the results from their initial position towards the "Si^0" region. This shift is due to a silicon-rich carbide where the excess silicon is present as a result of the reduction of the silicon oxide layer.

The "oxidized region" on the two-dimensional plot also undergoes a shift towards "Si^0" as a function of the reaction time. The shift is indicative of aluminosilicate formation [36]. A number of possible aluminosilicates are depicted on the plot; these include mullite, sillimanite and amorphous Al_2SiO_5, and their spectroscopic values are included in Table II. It is impossible to determine from the data which aluminosilicate is being formed. Further support for the formation of aluminosilicates comes from Fig. 6c where the O1s–Si2p BE splitting decreases from 429.5 to 428.7 eV as a function of time at 800° C. The splitting of 428.7 eV is in agreement with the splitting given in Table II for the aluminosilicates.

It is interesting to note that the C1s–Si2p splitting also decreases as a function of time at 800° C (Fig. 6a). The decrease from approximately 183.5 to 182.0 eV suggests an increase in the crystallinity of the substrate SiC [16], possibly due to the loss of the oxidation reaction products proposed by Kee *et al.* [34], during the current reaction.

On the aluminium two-dimensional chemical state plot, reaction at 800° C produces two new regions, notably the "Al_4C_3" region and the "oxidized Al" region. The region covered by the "oxidized Al" is typical of an aluminosilicate region and falls below the oxide and hydroxide regions [36, 43]. Reference aluminosilicates have been included on the diagram. The data of Fig. 6b are further evidence for the formation of aluminosilicate because the O1s–Al2p splitting decreases from 457.5 to 456.5 eV (Table II).

The spectroscopic results suggest that in the reaction of aluminium with SiC/SiO_2 a number of reaction products are formed which include aluminosilicate, Al_4C_3 and liquid solution of silicon in aluminium.

TABLE II XPS spectroscopic parameters of reference compounds

Compound	Al2p	Al(*KLL*)	α′	Si2p	Si(*KLL*)	α′	O1s–Si2p	O1s–Al2p
Al_4C_3	73.7	1390.7	1463.1	–	–	–	–	–
Amorphous*† Al_2O_3	74.7	1387.7	1461.3	–	–	–	–	457.7
α-Al_2O_3†	74.0	1387.7	1461.8	–	–	–	–	456.6
Amorphous§ SiO_2	–	–	–	103.2	1608.5	1711.7	429.4	–
Mullite‡	74.6	1386.9	1461.5	102.5	1609.5	1712.0	428.8	456.7
Sillimanite‡	74.7	1386.6	1461.3	102.5	1609.4	1711.9	429.1	456.9
Amorphous† Al_2SiO_5	74.8	1386.5	1461.3	102.6	1608.8	1711.4	428.9	456.7
SiC	–	–	–	100.2	1615.4	1715.6	–	–

*Grown on aluminium foil.
†Binding energy established by gold evaporation.
‡Binding energy established by C1s (adventitious) signal 284.6.
§Taken from [36].

3.1.2. Quantitative results

Figs 7 and 8 depict the results of the XPS quantitative analysis for three different oxide thickness; (i) no oxide (Figs 7a and 8a), (ii) a thin oxide (1.8 nm, Figs 7b and 8b) and (iii) a thick oxide (5.1 nm, Figs 7c and 8c). In Fig. 7, the data for the silicon in each phase normalized to the total silicon is plotted as a function of reaction time at 800° C. Fig. 8 is the analogous plot for the aluminium reaction products. In this diagram the aluminium from each component, normalized to the total silicon in the system, is plotted as a function of the reaction time at 800° C.

For the case where there is no oxide present on the SiC surface the reaction is simple. The aluminium reacts with SiC to form Al_4C_3 and free silicon as reaction products. This is shown by the decrease in the "SiC" component, the rise in the "Si" component (Fig. 7a) and the corresponding decrease in the "Al" component and rise in the Al_4C_3 component (Fig. 8a). The system has apparently reached equilibrium after approximately 60 min.

When there is a thin oxide (Figs 7b and 8b, Table II; experiment IV) there are the competing reactions of Al_4C_3 formation and oxidation reactions between aluminium and SiO_2. Within the first 10 min of reaction, silicon metal is detected and there is a decrease in the amount of SiO_2 and SiC (Fig. 7b). There is a corresponding increase in the amount of Al_4C_3 presumably as a result of the reaction of aluminium with SiC. There is also an increase in the oxidized aluminium phases from the reaction of alu-

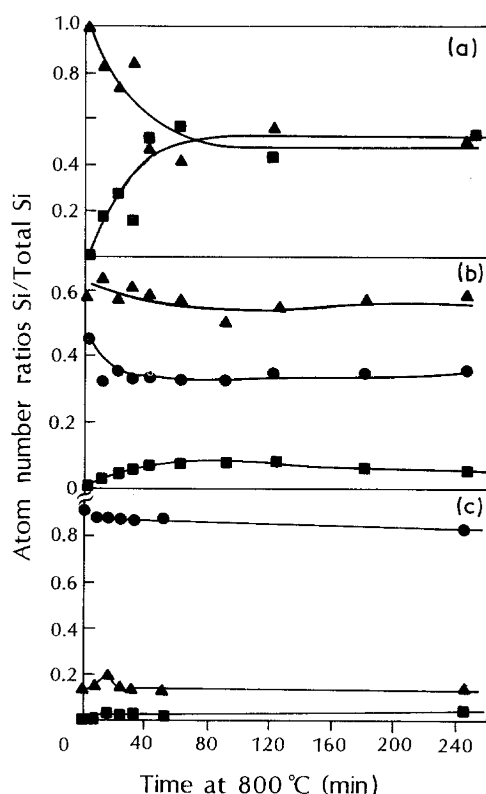

Figure 7 XPS atom number ratios for the different silicon components are plotted as a function of reaction time at 800° C for three different oxide thicknesses: (a) 0.0 nm, (b) 1.8 nm and (c) 5.1 nm. The components are (▲) SiC, (●) oxidized Si, (■) Si^0.

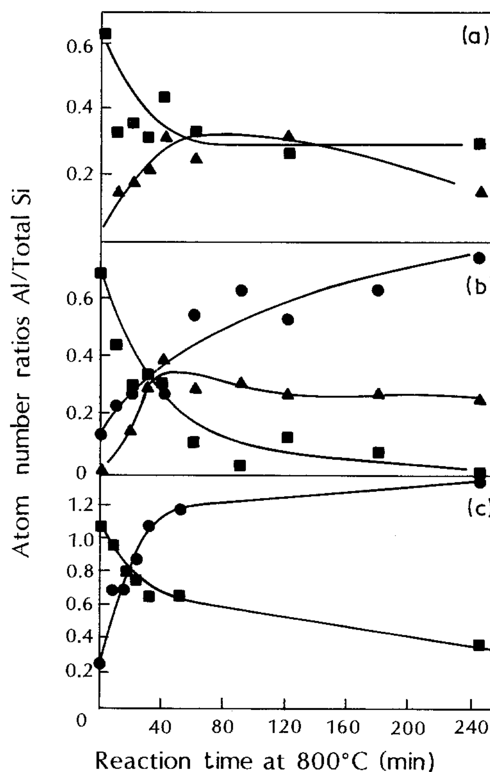

Figure 8 XPS atom number ratios for the different aluminium components are plotted as a function of reaction time at 800° C for three different oxide thicknesses: (a) 0.0 nm, (b) 1.8 nm and (c) 5.1 nm. The components are (▲) Al_4C_3, (●) oxidized aluminium, (■) Al^0. This graph is analogous to the silicon graph of Fig. 7.

minium with SiO_2 (Fig. 8b). The oxidized aluminium is in the form of alumina and aluminosilicates. The presence of oxidized silicon, however, must be due to aluminosilicate formation because the BE splitting between O1s–Si2p decreases to 102.8 eV.

The formation of Al_4C_3 appears to peak after approximately 60 min presumably due to liquid solution formation between silicon and aluminium inhibiting the further reaction of SiC with aluminium [44, 45]. After approximately 240 min reaction the aluminium metal is consumed, the Al_4C_3 is slowly decreasing and the oxidized aluminium component is still increasing. It is clear that at $t = 240$ min the system has not reached equilibrium; however, it is apparent that the only phases that will be present when equilibrium is obtained are alumina and/or aluminosilicates, metallic silicon and SiC.

When the oxide is thick ($d = 5.1$ nm, Figs 7c and 8c), the underlying carbide plays no role in the reaction. This observation is supported by the data of Fig. 6c, where the C1s–Si2p splitting for the thick oxide shows no change as a function of reaction time. Hence the data in Figs 7c and 8c indicate that the only possible reactions are redox reactions or aluminosilicate formation. In the first 20 min of reaction the "oxidized Si" component decreases presumably as a result of redox reaction between the aluminium and SiO_2. The redox reaction will produce Si^0, observed as the increase in the Si^0 component. Similarly the aluminium metal decreases at the expense of the "oxidized Al" component as a function of the reaction time.

The results depicted in Figs 7 and 8 relate only to the liquid and solid phase reaction products and do not include gaseous species. The XPS raw intensities as a function of reaction time provide an indirect method of assessing the amount of volatile species generated, because a decrease in the intensity emitted by any particular element represents a loss of that element from the surface. As no decrease was detected in the absolute intensity of silicon or aluminium it can be concluded that there was no significant loss of material by volatilization.

3.2. Thermodynamic modelling

In calculating the equilibrium chemical composition of a given system, an important assumption is that the system is homogeneous. This is not the case for the $Al/SiO_2/SiC$ system, which is inhomogeneous, because it contains two distinct reaction sites, i.e. the Al/SiO_2 and the SiO_2/SiC interfaces. The problem of inhomogeneity is to some extent alleviated because preliminary computations showed that SiO_2 and SiC do not react together at 800° C. Consequently, the problem is reduced to examining firstly the reactions at the Al/SiO_2 interface, and subsequently the reactions between SiC and the reaction products from reaction at the Al/SiO_2 interface.

In the model we have adopted to treat the inhomogeneous $Al/SiO_2/SiC$ system examined in the XPS experiment, we have taken a homogeneous mixture of SiO_2 and SiC in the molar ratio corresponding to that in the surface volume examined by XPS. The time dependence of the reaction measured in XPS has been

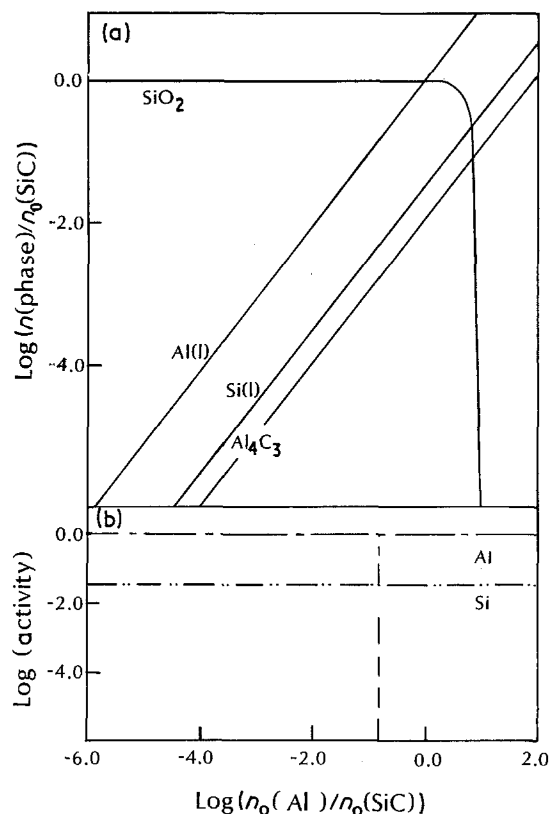

Figure 9 Reaction of aluminium with SiC at 800° C. (a) Phase quantities expressed as the logarithm of the molar ratio of the phase to initial SiC, plotted as a function of progress variable (defined in text). (b) Logarithm of the activities of the liquid components plotted as a function of the progress variable.

simulated by the stepwise addition of aluminium to the homogeneous mixture of SiO_2 and SiC. The progress variable is, therefore, defined as the logarithm of $n_0(Al)/n_0(SiC)$, where n_0 is the initial (pre-reaction) number of moles of the particular phase. In this way the presence of intermediate phases can be recognized before the bulk system attains equilibrium.

A further problem with the modelling arises from the evolution of gaseous species such as SiO(g), Al_2O(g) and CO(g). In the homogeneous system there will be a greater evolution of gases than in the inhomogeneous system, because the liquid aluminium layer provides a partial barrier to the loss of volatile reaction products. It has already been inferred from the XPS experiments that the loss of volatile reaction products is small. Prabriputaloong and Piggott [46] also found that volatile aluminium oxides are released only in small quantities during interfacial reactions between SiO_2 and thin film aluminium. For the purposes of the thermodynamic model the pressure of the system was made artificially high (10^{-4} atm) by comparison to the XPS experiments, in order to suppress the presence of a significantly large gas phase.

The results of the stepwise addition of liquid aluminium to SiC (β-phase) and SiO_2 (α-quartz) are depicted in Figs 9 to 11 in which $\log(n(\text{phase})/n_0(\text{SiC}))$ (number of moles of a given phase created or destroyed during the course of reaction) and log (activity) of liquid components are plotted against the progress variable. Three different SiO_2/SiC molar ratios were treated, representing the cases for (a) no oxide layer (Fig. 9), (b) a thin oxide layer of 0.118 mol

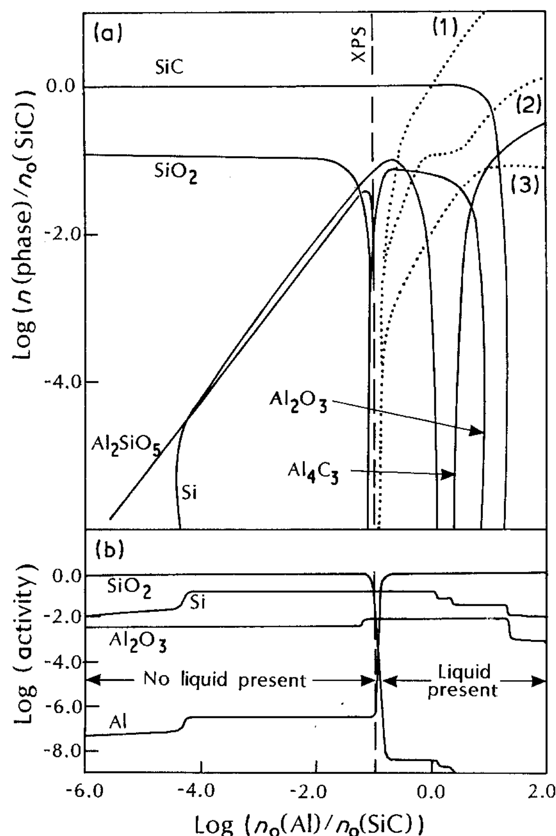

Figure 10 Reaction of aluminium with 0.118 mol SiO_2 and SiC at 800° C. The molar ratios of SiC to SiO_2 have been estimated from the XPS experiments and have been chosen to represent the thin oxide case. (a) Phase quantities expressed as the logarithm of the molar ratio of the phase to initial SiC plotted as a function of the progress variable (defined in text). (b) Logarithm of the activities of the liquid components plotted as a function of the progress variable. The vertical line is the estimated molar ratio of aluminium to SiC in the corresponding XPS experiment. The dashed lines are the liquid phases and are defined as (1) Al(l), (2) Si(l), (3) Al_2O_3(l).

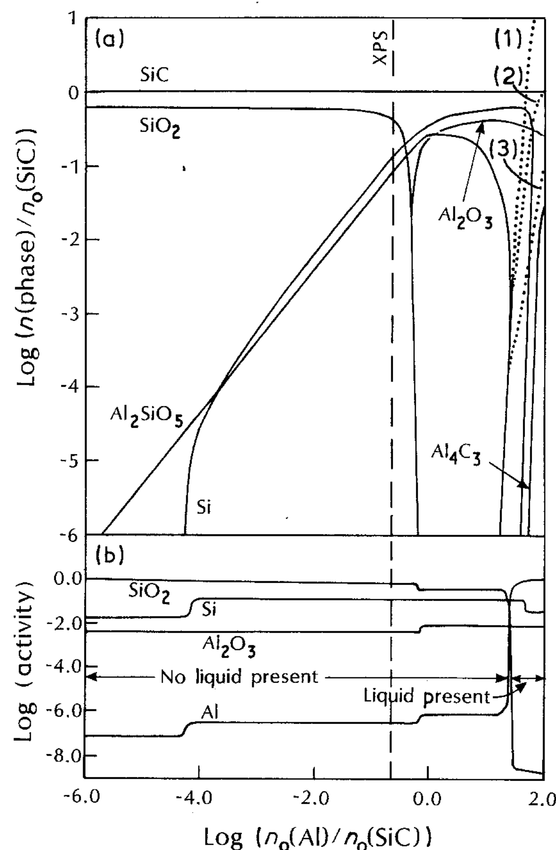

Figure 11 Reaction of aluminium with 0.629 mol SiO_2 and SiC at 800° C. The molar ratios of SiC to SiO_2 have been estimated from the XPS experiments and have been chosen to represent the thick oxide case. (a) Phase quantities expressed as the logarithm of the molar ratio of the phase to SiC plotted as a function of the progress variable (defined in text). (b) Logarithm of the activities of the liquid components plotted as a function of the progress variable. The vertical line is the estimated molar ratio of aluminium to SiC in the corresponding XPS experiment. The dashed lines are the liquid phases and are defined as (1) Al(l), (2) Si(l), (3) Al_2O_3(l).

SiO_2 (Fig. 10), and (c) a thick oxide layer of 0.629 mol SiO_2 (Fig. 11). (The quantities of SiO_2 were chosen to be representative of the actual values used in the XPS experiments and were taken from Table I, experiments I, IV and V.) In each case, a constant quantity of SiC was reacted (1.0 mol) and the amount of aluminium was varied in steps from approximately 10^{-6} to 100 mol. The vertical dashed line, labelled "XPS" appearing on each diagram represents the estimated reactant molar ratio of aluminium to SiC in the surface volume examined by XPS (see Table I).

The reaction sequence for the "no oxide" layer (Fig. 9) is quite straightforward: SiC reacts with aluminium to produce Al_4C_3 and Si(l). The activity of liquid silicon (Fig. 9b), which is virtually constant (0.037), is in agreement with previous observations [17, 44] that, during the reaction of SiC with liquid aluminium, that the activity of silicon in the liquid phase increases until it reaches a constant value at equilibrium, at which stage no more Al_4C_3 is produced.

In the case where a thin oxide layer is present (Fig. 10), the order of phases appearing with increasing addition of aluminium is Al_2SiO_5 (andalusite), Si(s) (once the SiO_2 is consumed), Al_2O_3 (α-phase) and finally Al_4C_3 (at which stage SiC begins to disappear). The equilibrium set of phases intersected by the XPS reactant molar ratio line comprise SiC, Si(s), Al_2SiO_5 and Al_2O_3.

There is no liquid phase present at equilibrium for the XPS reactant molar ratio. Note that the "no liquid present" region of Fig. 10b (and Fig. 11b) is included simply to display the overall changes in activities of the liquid phase components over the entire progress variable range. The sum of the activities of the liquid components is less than unity in this region, so the liquid phase does not physically exist. However, at slightly higher log (n_0(Al)/n_0(SiC)) values, a liquid phase appears which consists mainly of Al(l) with smaller amounts of Si(l) and Al_2O_3(l). The activities of the Si(l) and Al_2O_3(l) decrease rapidly once Al_4C_3 starts to form. The fact that liquid Al_2O_3 is present below its melting point is due to either the assumption of ideal mixing in the liquid phase (i.e. the activity coefficient should be less than unity) or else due to oxygen solubility in liquid aluminium.

At this point it should be emphasized that the equilibrium set of phases predicted by CHEMIX are those phases which are thermodynamically most stable, i.e. no account is taken of reaction kinetics. Hence, slow reaction rates may, in reality, preclude the formation of certain thermodynamically predicted phases and, instead, compositionally similar metastable phases

may be produced. As a test, some additional CHEMIX runs were performed with the suppression of the most thermodynamically stable phases in order to force metastable phases to appear in the output. The range of progress variable values over which metastable phases occur and the order of appearance of metastable phases are not significantly different from the results reported in this paper for the compositionally similar stable phases. Unfortunately, it was not possible to analyse the products of the XPS experiments, due to their very small quantities, in order to determine their exact phase compositions which would more accurately constrain thermodynamic modelling.

The sequence of phases appearing for a thick oxide layer (Fig. 11) is essentially the same as that for the thin oxide layer with the exception that the appearance of some of the phases (liquid phases and Al_4C_3) is shifted to higher values of the progress variable. The equilibrium set of phases intersected by the XPS reactant molar ratio line comprise SiC (essentially unreacted), SiO_2, Si(s) and Al_2SiO_5.

4. Discussion

The agreement between the equilibrium phase assemblages of the XPS experiments with those predicted by thermodynamic modelling is generally quite good. Further, the modelling provides thermodynamic evidence that supports the XPS conclusions that aluminosilicate and Al–Si liquid solutions are present at the reacted interface.

For the "no oxide" case, both methods resulted in an equilibrium phase assemblage consisting of SiC, Al(l), Si(l) and Al_4C_3 (Figs 8a, 9a and 10a).

Similarly there is good agreement between the equilibrium results for the thin oxide case, but there is a discrepancy in the nature of the intermediate phases. Specifically, Al_4C_3 was observed early in the XPS experiments, in coexistence with Al_2O_3 and aluminosilicate (Fig. 8b). Fig. 10a shows that Al_4C_3 cannot stably coexist with both Al_2SiO_5 and Al_2O_3 and only begins to appear at high log $(n_0(\text{Al})/n_0(\text{SiC}))$ values in the absence of SiO_2. A possible explanation for this inconsistency may be provided by localized fluctuations in the thickness of the SiO_2 layer [47] which enables aluminium to react with SiC to produce Al_4C_3 in regions where there is little oxide present, whereas only oxidized aluminium phases are being produced in areas where the oxide layer is thicker. As the overall system approaches equilibrium, Al_4C_3 is consumed to produce the thermodynamically stable Al_2SiO_5 and Al_2O_3.

The appearance of a liquid phase consisting predominantly of Al(l) with minor amounts of Si(l) at progress variable values slightly higher than the XPS reactant molar ratio (Fig. 11a) is also evident in the XPS silicon data (Fig. 5) which indicates that there is some solid solution formation between aluminium and silicon.

In the case of the thick oxide layer (Fig. 11), the equilibrium phase assemblage intersected by the XPS reactant molar ratio line, comprising SiC (essentially unreacted), SiO_2, Si(s) and Al_2SiO_5, is again in good agreement with the observed XPS results. The XPS results of Fig. 6a indicate that the SiC remains essentially unreacted because the C1s–Si2p splitting remains constant as a function of increasing reaction time. Si^0 is observed early in the reaction and the aluminium oxidizes rapidly to produce aluminosilicate as demonstrated by the data for the aluminium two-dimensional chemical state plot (Fig. 5).

5. Conclusions

X-ray photoelectron spectroscopy and thermodynamic modelling have demonstrated that three distinct regimes exist in the $Al/SiO_2/SiC$ system. First, there is the clean SiC surface, where reaction with aluminium will produce Al_4C_3. Second, there is the thin oxide regime, e.g. native oxide, which may be patchy and although reaction at 800° C will produce oxidized aluminium products the patchiness of the oxide still allows for the production of Al_4C_3. Third, is the thick oxide regime, which clearly exists at 5.0 nm, where reaction at 800° C produces only oxidized aluminium phases. It is this third regime which is of importance to the manufacture of Al–SiC composite materials because in this case deleterious reaction products such as Al_4C_3 are not present. It is, however, unclear from our experiments whether the presence of the oxidized aluminium reaction phases provides a barrier to further reaction with the SiO_2 layer or whether reaction proceeds until the SiO_2 is consumed at which point Al_4C_3 would begin to be formed. If reaction does proceed until the SiO_2 is consumed then the time of mixing of SiC fibres in molten aluminium becomes an important parameter.

Acknowledgements

We thank S. Hardin for help in the preparation of the precursor material for the aluminosilicates, Dr D. Hay for generating X-ray diffraction patterns of the reference materials, and Drs A. G. Turnbull and V. J. Wall for useful suggestions regarding the thermodynamic analysis. The manuscript has benefitted from the critical reviews of Drs M. J. Bannister, A. G. Turnbull, M. B. Trigg and H. G. Scott.

References

1. E. PETTENPAUL, W. VON MUNCH and G. ZIEGLER, *Inst. Phys. Conf. Ser.* **53** (1980) 21.
2. M. L. TORTI, R. A. ALLIEGRO, D. W. RICHERSON, M. C. WASHBURN and G. Q. WEAVER, *Proc. Brit. Ceram. Soc.* **22** (1973) 129.
3. C. VAN OPDORP, *Solid State Electron.* **14** (1971) 613.
4. W. V. MUNCH, W. KURZINGER and I. PFAFFENEDER, *ibid.* **19** (1976) 871.
5. A. SUZUKI, H. ASHIDA, N. FURUI, K. MAMENO and H. MATSUNAMI, *Jpn J. Appl. Phys.* **21** (1982) 579.
6. E. GUGEL, in "Engineering Applications of Ceramic Materials", edited by M. M. Schwartz (American Society for Metals, Metals Park, Ohio, 1985) pp. 117–125.
7. S. TOWATA and S. YAMADA, *J. Jpn Inst. Metals* **47** (1983) 159.
8. S. J. BARCLAY, J. R. FOX and H. K. BOWEN, *J. Mater. Sci.* **22** (1987) 4403.
9. J. A. CORNIE, R. S. SUPLINSKAS and A. W. HAUZE, *Ceram. Engng Sci. Proc.* **1** (1980) 728.
10. S. R. NUTT and F. E. WAWMER, *J. Mater. Sci.* **20** (1985) 1953.

11. T. N. TAYLOR and D. S. PHILLIPS, *J. Vac. Sci. Technol.* **A6** (1988) 982.
12. M. N. RAHAMAN and L. C. DE JONGHE, *Am. Ceram. Soc. Bull.* **66** (1987) 782.
13. W. C. HARRIGAN, *Metall. Trans.* **9A** (1978) 503.
14. R. J. ARSENAULT and C. S. PANDE, *Scripta Metall.* **18** (1984) 1131.
15. V. M. BERMUNDEZ, *Appl. Phys. Lett.* **42** (1983) 70.
16. L. PORTE, *J. Appl. Phys.* **60** (1986) 635.
17. T. ISEKI, T. KAMEDA and T. MARUYAMA, *J. Mater. Sci.* **19** (1984) 1692.
18. A. I. AKINWANDE and J. D. PLUMMER, *J. Electrochem. Soc.* **134** (1987) 2297.
19. P. T. B. SHAFFER, *Acta Crystallogr.* **B25** (1969) 477.
20. B. E. DEAL and A. S. GROVE, *J. Appl. Phys.* **36** (1965) 3770.
21. C. D. WAGNER and J. A. TAYLOR, *J. Electron. Spectrosc. Relat. Phenom.* **20** (1980) 83.
22. J. H. SCOFIELD, *ibid.* **8** (1976) 129.
23. A. E. HUGHES and B. A. SEXTON, *ibid.* **46** (1988) 31.
24. A. SAVITZKY and M. J. E. GOLAY, *Anal. Chem.* **36** (1964) 1627.
25. J. STEINER, Y. TERMONIA and J. DELTOUR, *ibid.* **44** (1972) 190.
26. A. PROCTER and P. M. A. SHERWOOD, *Anal. Chem.* **54** (1982) 13.
27. L. NYBORG, A. NYLUND and I. OLEFJORD, *SIA Surf. Interface Anal.* **12** (1988) 110.
28. S. TANUMA, C. J. POWELL and D. R. PENN, *Surf. Sci.* **192** (1987) L849.
29. A. G. TURNBULL and M. W. WADSLEY, The Australian Institute of Mining and Metallurgy Symposium on Extractive Metallurgy, Melbourne (1984) p. 78.
30. J. HEDMAN, Y. BAER, A. BERNDTSSON, M. KLASSON, G. LEONHARDT, R. NILSSON and C. NORDLING, *J. Electron. Spectrosc. Relat. Phenom.* **1** (1972/73) 101.
31. Y. TAJIMA, K. KIJIMA and W. D. KINGERY, *J. Chem. Phys.* **77** (1982) 2592.
32. J. DERRIEN and F. RINGEISEN, *Solid State Commun.* **50** (1984) 627.
33. H. HOECHST and M. TANG, *J. Vac. Sci. Technol.* **A5** (1987) 1640.
34. R. W. KEE, K. M. GEIB, C. W. WILMSEN and D. K. FERRY, *ibid.* **15** (1978) 1520.
35. T. W. HICKMOTT, *J. Appl. Phys.* **51** (1980) 4269.
36. C. D. WAGNER, D. E. PASSOJA, H. F. HILLERY, T. G. KINISKY, H. A. SIX, W. T. JANSEN and J. A. TAYLOR, *J. Vac. Sci. Technol.* **21** (1982) 933.
37. Y. MIZOKAWA, K. M. GEIB and C. W. WILMSEN, *ibid.* **A4** (1986) 1696.
38. L. PORTE and A. SARTRE, *J. Mater. Sci.* **24** (1989) 271.
39. J. JORGENSEN, M. E. WADSWORTH and I. B. CASTLER, *J. Amer. Ceram. Soc.* **42** (1959) 613.
40. Y. N. SUN, A. FELDMAN and E. N. FARABAUGH, *Thin Solid Films* **157** (1988) 351.
41. M. DEL GIUDICE, J. J. JOYCE and J. H. WEAVER, *Phys. Rev. B.* **36** (1987) 4761.
42. L. J. BRILLSON, A. D. KATNANI, M. KELLY and G. MARGARITONDO, *J. Vac. Sci. Technol.* **A2** (1984) 551.
43. R. BICKER, H. DEGER, W. HERZOG, K. RIESER, H. PLUM, G. HOHLNEICHER and H. J. FREUND, *J. Catal.* **94** (1985) 69.
44. A. S. ISAIKIN, V. M. CHUBAROV, B. F. TREFILOV, V. A. SILAEV and YU. A. GORELOV, *Met. Sci. Heat Treatment* (translated from *Metall. Termich. Obrabotka Metallov*) **22** (1980) 815.
45. A. E. GERSHINSKII, A. A. KHOROMENKO and F. L. EDELMAN, *Phys. Status Solidi (a)* **25** (1974) 645.
46. K. PRABRIPUTALOONG and M. R. PIGGOTT, *J. Electrochem.* **121** (1974) 430.
47. A. H. CARIM and A. BHATTACHARYYA, *Appl. Phys. Lett.* **46** (1985) 872.

Received 20 June
and accepted 1 December 1989